Hindawi Publishing Corporation
Journal of Nanomaterials
Volume 2015, Article ID 151740, 5 pages
http://dx.doi.org/10.1155/2015/151740

Research Article

Magnetic Force Microscopy Study of Zr_2Co_{11}-Based Nanocrystalline Materials: Effect of Mo Addition

Lanping Yue,[1] Yunlong Jin,[1,2] Wenyong Zhang,[1,2] and David J. Sellmyer[1,2]

[1]*Nebraska Center for Materials and Nanoscience, University of Nebraska, Lincoln, NE 68588, USA*
[2]*Department of Physics and Astronomy, University of Nebraska, Lincoln, NE 68588, USA*

Correspondence should be addressed to Lanping Yue; lyue2@unl.edu

Received 8 May 2015; Accepted 21 July 2015

Academic Editor: Mohmmad A. Malik

Copyright © 2015 Lanping Yue et al. This is an open access article distributed under the Creative Commons Attribution License, which permits unrestricted use, distribution, and reproduction in any medium, provided the original work is properly cited.

The addition of Molybdenum was used to modify the nanostructure and enhance coercivity of rare-earth-free Zr_2Co_{11}-based nanocrystalline permanent magnets. The effect of Mo addition on magnetic domain structures of melt spun nanocrystalline $Zr_{16}Co_{84-x}Mo_x$ ($x = 0$, 0.5, 1, 1.5, and 2.0) ribbons has been investigated. It was found that magnetic properties and local domain structures are strongly influenced by Mo doping. The coercivity of the samples increases with the increase in Mo content ($x \leq 1.5$). The maximum energy product $(BH)_{max}$ increases with increasing x from 0.5 MGOe for $x = 0$ to a maximum value of 4.2 MGOe for $x = 1.5$. The smallest domain size with a relatively short magnetic correlation length of 128 nm and largest root-mean-square phase shift Φ_{rms} value of 0.66° are observed for the $x = 1.5$. The optimal Mo addition promotes magnetic domain structure refinement and thus leads to a significant increase in coercivity and energy product in this sample.

1. Introduction

Nanocrystalline Zr_2Co_{11}-based materials are promising candidates for the development of rare-earth-free permanent magnets due to their good intrinsic magnetic properties with strong uniaxial anisotropy (11 Merg cm^{-3}) and high Curie temperature (>500°C) [1–6]. The rhombohedral Zr_2Co_{11} phase is identified to be responsible for the magnetic hardness in rapidly quenched alloys as discussed elsewhere [6–9]. The coercivity and maximum energy product of Zr_2Co_{11}-based nanocrystalline materials also were efficiently enhanced by the introduction of Mo element [10, 11]. The investigation of the magnetic microstructure and property relationship is important for the understanding of these improvements and, more generally, for the development of high-performance magnets. So far, how element additions affect magnetic microstructure and what is the correlation of magnetic microstructure and magnetism are still unclear.

In this work, how Mo addition affects the magnetic domain structures of nanocrystalline $Zr_{16}Co_{84-x}Mo_x$ ($x = 0, 0.5, 1.0, 1.5$, and 2) alloys has been analyzed by Magnetic Force Microscopy (MFM). MFM provides the capability of observing magnetic domains with spatial resolutions down to 10 nm or better. It allows us to study in detail the evolution of local magnetic domain structures of Zr_2Co_{11}-based alloys with Mo additions and thus helps us to understand the magnetic microstructure-property relationship and further optimize the magnetic properties of such nanocrystalline materials.

2. Materials and Methods

$Zr_{16}Co_{84-x}Mo_x$ ($x = 0, 0.5, 1, 1.5$, and 2.0) alloys were prepared by arc melting of high-purity elements. The ingots were subsequently melt-spun in an argon atmosphere by ejecting molten ingots in a quartz tube onto the surface of a copper wheel with a rotating speed of 55 m/s. The obtained ribbons have typical size of 2 mm wide and 50 μm thick. The elemental compositions of the samples were determined by FEI Nova NanoSEM 450 equipped with an Energy Dispersive X-ray Spectrometer (EDS) to confirm the amount of Mo dopant. The SEM/EDS results identified Mo contents (atomic %) are 0.94, 1.32, and 1.87 for the samples $x = 1, 1.5$, and 2, respectively, which are slightly smaller than the nominal concentration. For the simplicity, we still use $x = 1, 1.5$, and 2 here to represent these samples in the paper.

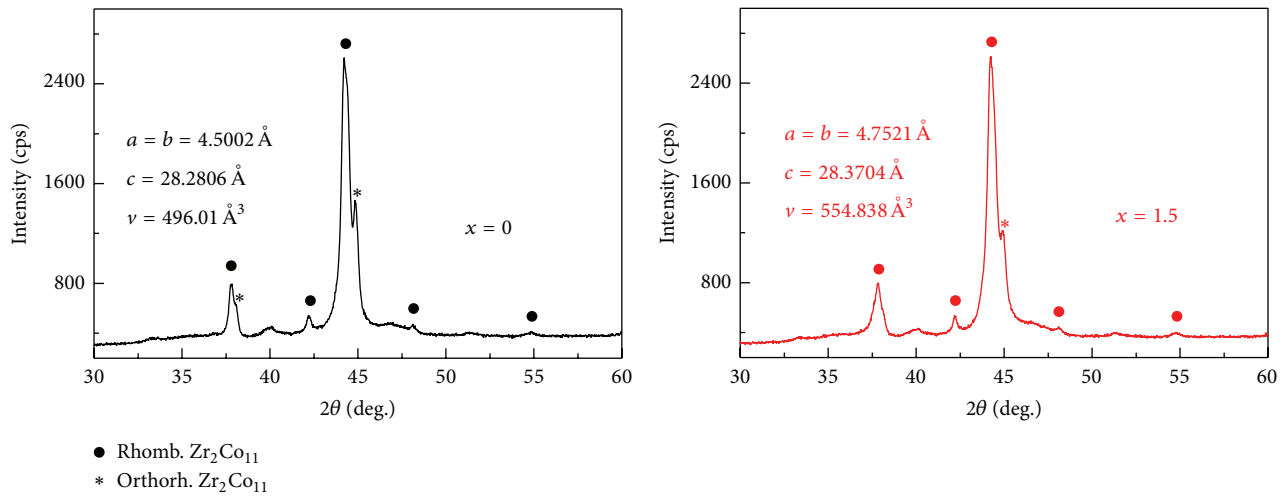

FIGURE 1: XRD patterns of the nanocrystalline $Zr_{16}Co_{84-x}Mo_x$ ($x = 0$ and 1.5).

The phase components of nanocrystalline $Zr_{16}Co_{84-x}Mo_x$ ($x = 0$ and 1.5) were examined by a Rigaku D/Max-B X-ray diffractometer (XRD) with Co K_α radiation. As shown in the XRD patterns (Figure 1), the diffraction peaks of the samples are identified as rhombohedral Zr_2Co_{11} and orthorhombic Zr_2Co_{11} structures. The relative intensity of the diffraction peaks of rhombohedral Zr_2Co_{11} for $x = 1.5$ is higher than that for $x = 0$, while the orthorhombic Zr_2Co_{11} peaks decrease with Mo addition, indicating that Mo addition increases the volume fraction of the rhombohedral phase. The sample with $x = 1.5$ mainly consists of the hard magnetic rhombohedral Zr_2Co_{11} nanostructure.

The magnetic hysteresis loops were measured by a Superconducting Quantum Interference Device (SQUID) magnetometer with the maximum applied field of 7 T parallel to the length direction of ribbons at room temperature. The magnetic domain structures of samples were investigated in detail at the micron to nanometer scales by Bruker-ICON Magnetic Force Microscopy (MFM). All the samples are thermally demagnetized. The MFM uses a magnetic tip to measure the magnetic force gradient distribution on a sample's surface by oscillating the cantilever normal to the surface at its resonant frequency. The magnetization of the Co-Pt MFM tip with high coercivity and high lateral resolution is perpendicular to the sample surface and points downward. All the MFM images were obtained at the same lift scan height of 20 nm, using the tapping/lift mode at room temperature.

3. Results and Discussion

Figure 2 shows hysteresis loops of the nanocrystalline $Zr_{16}Co_{84-x}Mo_x$ ($x = 0, 1.5$, and 2.0) alloys at room temperature. It is evident that Mo addition improves the rectangularity shape of the hysteresis loop and increases the coercivity from 0.6 kOe for $x = 0$ to 2.9 kOe for $x = 1.5$. This leads to a significant increase of the maximum energy product $(BH)_{max}$. The best maximum energy product at room

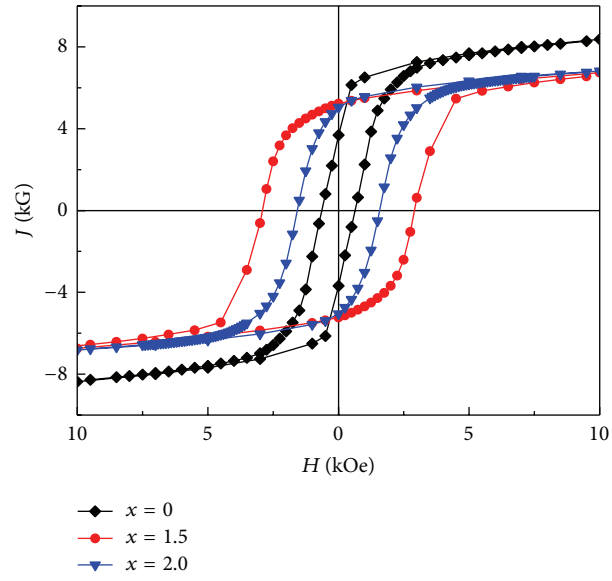

FIGURE 2: The hysteresis loops of the nanocrystalline $Zr_{16}Co_{84-x}Mo_x$ ($x = 0$, 1.5, and 2.0) alloys at room temperature.

temperature of 4.2 MGOe has been achieved for the $x = 1.5$ sample, and then it decreases with excessive Mo addition ($x = 2$) due to the decrease of coercivity.

The magnetic properties (coercivity H_c, anisotropy field H_a, and maximum energy product $(BH)_{max}$) of four samples ($x = 0, 1, 1.5$, and 2) deduced from hysteresis loops are listed in Table 1. The coercivity, anisotropy field, and maximum energy product are found to strongly depend on the Mo content. As discussed by Jin et al. [9], Mo addition increases the volume fraction of the hard magnetic phase, decreases the grain size of soft magnetic phase, and promotes the interphase exchange coupling action between hard magnetic and soft magnetic grains. The magnetocrystalline anisotropy field $H_a = 2K/M_0$ and the spontaneous magnetization M_0 can be determined by fitting the high-field part of

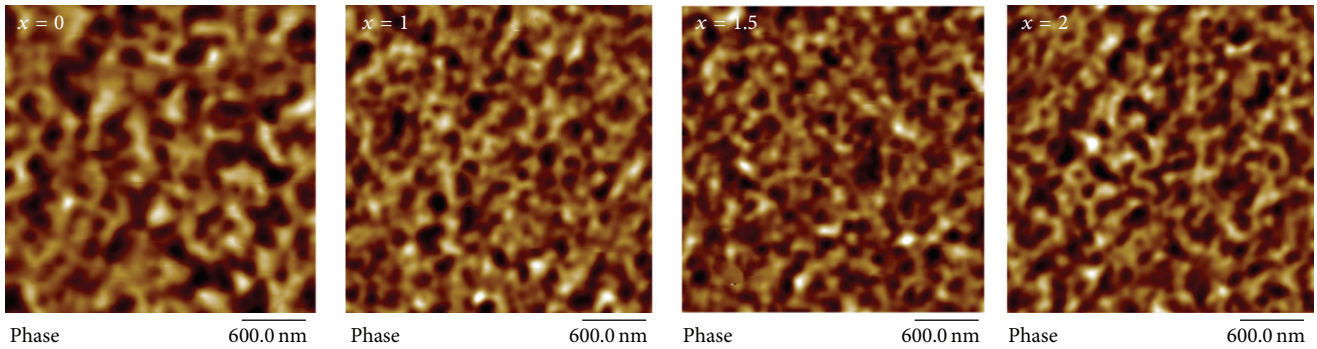

Figure 3: Typical magnetic domain structures of nanocrystalline $Zr_{16}Co_{84-x}Mo_x$ samples with $x = 0, 1, 1.5$, and 2. Each image is 3 μm × 3 μm in size.

Table 1: Dependence of the magnetic properties (coercivity H_c, anisotropy field H_a, and maximum energy product $(BH)_{max}$) and of the parameters of MFM images (root-mean-square values Φ_{rms} of the phase shift of the images and average magnetic correlation length L) on the Mo content x in nanocrystalline $Zr_{16}Co_{84-x}Mo_x$ (x = 0, 1, 1.5, and 2.0) ribbons.

Mo(x)	H_c (kOe)	H_a (kOe)	$(BH)_{max}$ (MGOe)	Φ_{rms} (°)	L (nm)
$x = 0$	0.6	18	0.5	0.13	225
$x = 1$	2.1	23	2.6	0.63	154
$x = 1.5$	2.9	29	4.2	0.66	128
$x = 2$	1.6	22	2.3	0.57	203

the hysteresis loops using the law of approach to saturation method [12]. As shown in Table 1, the coercivity increases with increasing Mo content and reaches the maximum value of 2.9 Oe when $x = 1.5$. This is possibly due to the large increase of the anisotropy field of the hard magnetic phase from 18 kOe for $x = 0$ to 29 kOe for $x = 1.5$. This leads to a significant increase of the maximum energy product from 0.5 MGOe for $x = 0$ to 4.2 MGOe for $x = 1.5$.

Figure 3 shows the typical magnetic domain structures of $Zr_{16}Co_{84-x}Mo_x$ samples with $x = 0, 1, 1.5$, and 2. All of these MFM images show bright-dark domain patterns with sharp contrast. The MFM image contrast represents magnetic force gradient mapping. Many magnetic grains participate in the formation of an interaction domain in which the grains exhibit the similar orientation of magnetization (up-down domains). Such domain patterns are well known to describe ferromagnetic structures [13]. Magnetic measurement results also indicate that all the samples are ferromagnetic at room temperature. From these MFM images we see that the domain size is on the nanometer scale and varies nonmonotonically with Mo content. It is easy to define the average domain size for simple domain configurations by visual methods. But for the complicated irregular interaction domains the magnetic correlation length L (the average domain width) can be estimated by several methods [13–17]. We have used the grain-size-analysis software incorporated in our MFM system to calculate L from the MFM images as an average over the lateral dimension of the domains sizes. The mean values of L determined from each MFM image are 225 nm, 154 nm, 128 nm, and 203 nm for $x = 0, 1, 1.5$, and 2, respectively, as shown in Table 1. The given L values represent an average of magnetic domains in three 3 μm × 3 μm MFM images taken at various places on each sample surface. For the $x = 1.5$ sample, the domains show a more even size distribution with the relatively smaller domain size, while larger domains were observed for the $x = 0$ sample.

The magnetic correlation length L is basically related to the intergrain exchange coupling. The short magnetic correlation length indicates the formation of smaller magnetic domains, which is due to weaker intergrain exchange coupling among hard magnetic grains. So refinement of magnetic domain structure for the $x = 1.5$ sample can be well understood. The improvement of the maximum energy product of the samples upon the Mo addition can therefore be attributed to the refinement of the magnetic microstructure arising from the weaker intergrain exchange coupling action.

The MFM image measures the phase lag between the drive voltage and the cantilever response. Magnetic attractive/repulsive forces cause shifts of both the resonance frequency and the phase. The phase image contrast represents magnetic force gradient mapping. Vertical gradients in the magnetic force cause a shift Δf_0 in the resonance frequency. In this case, the drive frequency shifts lead to phase shifts $\Delta\Phi$ which then gives an image of the magnetic force gradients. The root-mean-square value of phase shift Φ_{rms} of the MFM images is the standard deviation of the phase shift Φ within the given scan area and it can be calculated by the following equation [18]:

$$\Phi_{rms} = \sqrt{\frac{\sum_{i=1}^{N} \left(\Phi_i - \Phi_{ave}\right)^2}{N}}. \quad (1)$$

Here Φ_{ave} is the average Φ value within the scan area of the MFM image, Φ_i is the current ith Φ value, and N is the number of points within a given area.

The values of Φ_{rms} of the MFM images of $Zr_{16}Co_{84-x}Mo_x$ samples ($x = 0, 1, 1.5$, and 2) are listed in Table 1. Generally, the evolution of Φ_{rms} of the MFM images can be used to indicate the variation of the magnetic properties of the samples. It seems that there is a clear-cut correlation between Φ_{rms} and coercivity H_c or maximum energy product. The highest Φ_{rms} value of 0.66° for the sample with $x = 1.5$

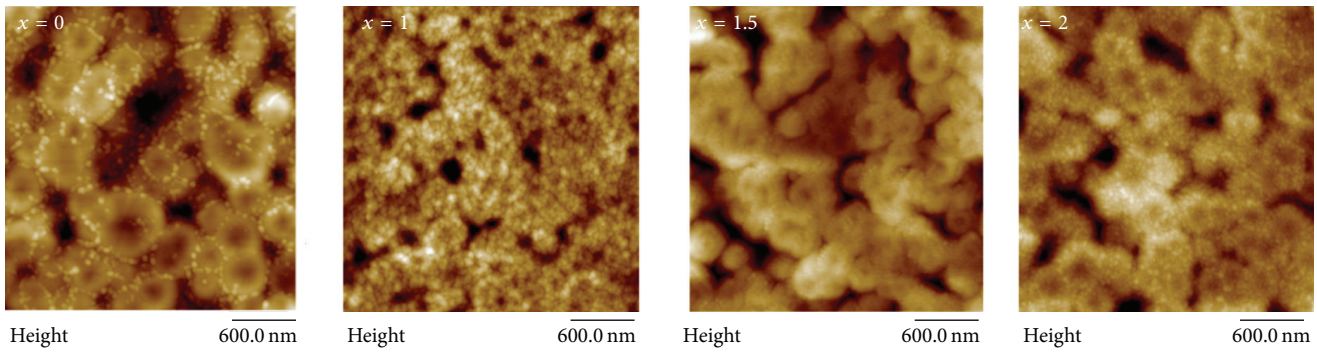

FIGURE 4: Atomic force microscopy (AFM) images of nanocrystalline $Zr_{16}Co_{84-x}Mo_x$ samples with $x = 0, 1, 1.5$, and 2. Each image is 3 μm × 3 μm in size.

is in good agreement with the largest coercivity of 2.9 kOe and the highest maximum energy product $(BH)_{max}$ value of 4.2 MGOe. We find that the smaller the domain sizes and the larger the phase shift Φ_{rms} values the better the magnetic properties of the samples. This corresponds to a maximum energy product enhancement via improved magnetic domain refinement. The results indicate that the refinement and uniformity of the magnetic microstructure, small magnetic domain size, and weak intergrain exchange coupling play important roles in the achievement of better magnetic properties.

Atomic force microscopy (AFM) images show topographic information of sample surfaces (Figure 4), which provides complementary information to the corresponding MFM images (Figure 3). In order to know whether there is a correlation between the sample surface roughness and the transition width of the magnetization of domains, the root-mean-square surface roughness (RMS) has been calculated from AFM images. The results indicate RMS roughness is 8.1 nm, 3.1 nm, 5.4 nm, and 7.4 nm for $x = 0, 1, 1.5$, and 2, respectively. It seems that there is no direct relationship between the magnetic domain sizes and the surface roughness of the samples, whereas the surface roughness of the samples with $x = 1$ and 1.5 is relatively smaller than that of the other two samples with $x = 0$ and $x = 2$. It suggests that suitable Mo addition leads to the formation of a smooth surface and thus narrows the grain size distribution, which may be favorable for the improvement of magnetic properties of such nanocrystalline Zr_2Co_{11}-based materials.

4. Conclusions

The effect of Mo addition on magnetic domain structures of nanocrystalline $Zr_{16}Co_{84-x}Mo_x$ ($x = 0, 1, 1.5$, and 2) ribbons was investigated by Magnetic Force Microscopy. We find that element addition is a feasible way to modify magnetic domain structure and enhance coercivity for $Zr_2(Co, Mo)_{11}$ nanocrystalline alloys. The best magnetic properties were obtained with a significant increase in coercivity and isotropic maximum energy product for the $x = 1.5$ sample. The short magnetic correlation length of 128 nm and larger root-mean-square phase shift value of 0.66 were observed for this sample. The above results indicate that proper Mo addition weakens intergrain exchange coupling among hard magnetic grains helping in the refinement of the magnetic domain structure and thus leads to the enhancement of the coercivity and the maximum energy product of this class of rare-earth-free nanocrystalline permanent magnet materials.

Conflict of Interests

The authors declare that there is no conflict of interests regarding the publication of this paper.

Acknowledgments

This research has been supported by DOE/Ames/BREM under Grant no. DE-AC02-07CH11358 and ARO (WF911NF-10-2-0099). The work was performed in part in facilities of Nebraska Center for Materials and Nanoscience, which is supported by The Nebraska Research Initiative.

References

[1] T. Ishikawa and K. Ohmori, "Hard magnetic phase in rapidly quenched Zr-Co-B alloys," *IEEE Transactions on Magnetics*, vol. 26, no. 5, pp. 1370–1372, 1990.

[2] C. Gao, H. Wan, and G. C. Hadjipanayis, "High coercivity in non-rare-earth containing alloys," *Journal of Applied Physics*, vol. 67, no. 9, pp. 4960–4962, 1990.

[3] E. Burzo, R. Grössinger, P. Hundegger et al., "Magnetic properties of $ZrCo_{5.1-x}Fe_x$ alloys," *Journal of Applied Physics*, vol. 70, no. 10, pp. 6550–6552, 1991.

[4] H. H. Stadelmaier, T. S. Jang, and E.-T. Henig, "What is responsible for the magnetic hardness in Co-Zr(-B) alloys?" *Materials Letters*, vol. 12, no. 5, pp. 295–300, 1991.

[5] B. Balasubramanian, B. Das, R. Skomski, W. Y. Zhang, and D. J. Sellmyer, "Novel nanostructured rare-earth-free magnetic materials with high energy products," *Advanced Materials*, vol. 25, no. 42, pp. 6090–6093, 2013.

[6] W. Y. Zhang, X. Z. Li, S. Valloppilly, R. Skomski, J. E. Shield, and D. J. Sellmyer, "Magnetism of rapidly quenched rhombohedral Zr_2Co_{11}-based nanocomposites," *Journal of Physics D: Applied Physics*, vol. 46, no. 13, Article ID 135004, 2013.

[7] G. V. Ivanova and N. N. Shchegoleva, "The microstructure of a magnetically hard Zr_2Co_{11} alloy," *Physics of Metals and Metallography*, vol. 107, no. 3, pp. 270–275, 2009.

[8] B. G. Demczyk and S. F. Cheng, "Structures of Zr_2Co_{11} and $HfCo_7$ intermetallic compounds," *Journal of Applied Crystallography*, vol. 24, no. 6, pp. 1023–1026, 1991.

[9] Y. L. Jin, W. Y. Zhang, R. Skomski, S. Valloppilly, J. E. Shield, and D. J. Sellmyer, "Phase composition and nanostructure of Zr_2Co_{11}-based alloys," *Journal of Applied Physics*, vol. 115, no. 17, Article ID 17A739, 2014.

[10] J.-B. Zhang, Q.-W. Sun, W.-Q. Wang, and F. Su, "Effects of Mo additive on structure and magnetic properties of $Co_{82}Zr_{18}$ alloy," *Journal of Alloys and Compounds*, vol. 474, no. 1-2, pp. 48–51, 2009.

[11] W. Y. Zhang, S. R. Valloppilly, X. Z. Li, R. Skomski, J. E. Shield, and D. J. Sellmyer, "Coercivity enhancement in Zr_2Co_{11}-based nanocrystalline materials due to Mo addition," *IEEE Transactions on Magnetics*, vol. 48, no. 11, pp. 3603–3605, 2012.

[12] G. C. Hadjipanayis, D. J. Sellmyer, and B. Brandt, "Rare-earth-rich metallic glasses. I. Magnetic hysteresis," *Physical Review B*, vol. 23, no. 7, pp. 3349–3354, 1981.

[13] L. Yue and S.-H. Liou, "Magnetic force microscopy studies of magnetic features and nanostructures," in *Scanning Probe Microscopy in Nanoscience and Nanotechnology 2*, B. Bhushan, Ed., NanoScience and Technology, chapter 10, pp. 287–319, Springer, Berlin, Germany, 2011.

[14] A. Hubert and R. Schäfer, *Magnetic Domains: The Analysis of Magnetic Microstructures*, Springer, 1998.

[15] M. V. Rastei, S. Colis, and J. P. Bucher, "Growth control of homogeneous pulsed electrodeposited Co thin films on n-doped Si(1 1 1) substrates," *Chemical Physics Letters*, vol. 417, no. 1–3, pp. 217–221, 2006.

[16] W. Szmaja, J. Grobelny, M. Cichomski, S. Hirosawa, and Y. Shigemoto, "Magnetic force microscopy investigation of the domain structure of nanocomposite $Nd_2Fe_{14}B/Fe_3B$ magnets," *Acta Materialia*, vol. 59, no. 2, pp. 531–536, 2011.

[17] Y. Fang, X. Yin, R. Zhao et al., "Magnetic micro-structural uniformity of die-upset Nd-Fe-B magnets," *Journal of Applied Physics*, vol. 111, no. 7, 2012.

[18] Digital Instruments. Veeco Metrology Group, *Scanner Probe Microscopy Training Notebook, Version 3.0*, Digital Instruments, Veeco Metrology Group, Santa Barbara, Calif, USA, 2000.

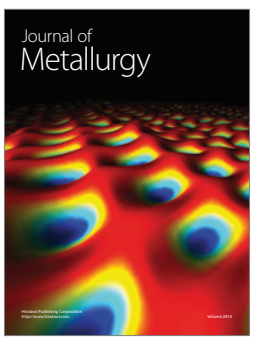

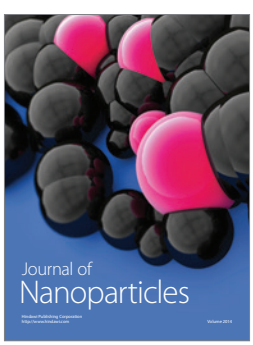

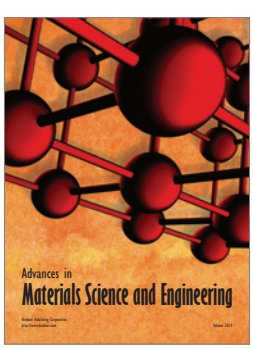

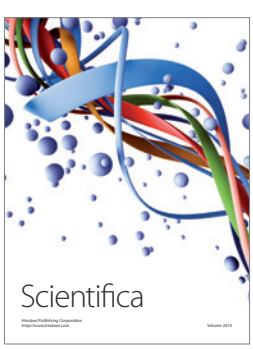

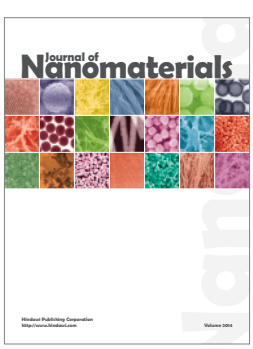

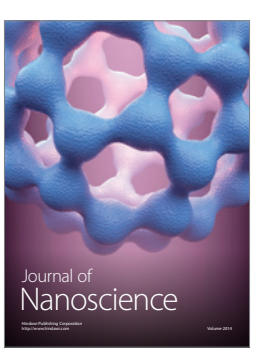

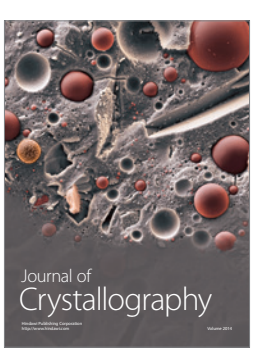

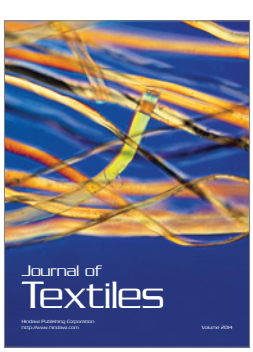

Hindawi

Submit your manuscripts at
http://www.hindawi.com